

Measurement of the $e^+e^- \rightarrow p\bar{p}$ cross section in the energy range from 3.0 to 6.5 GeV

J. P. Lees, V. Poireau, and V. Tisserand
*Laboratoire d'Annecy-le-Vieux de Physique des Particules (LAPP),
Université de Savoie, CNRS/IN2P3, F-74941 Annecy-Le-Vieux, France*

E. Grauges
Universitat de Barcelona, Facultat de Física, Departament ECM, E-08028 Barcelona, Spain

A. Palano^{ab}
INFN Sezione di Bari^a; Dipartimento di Fisica, Università di Bari^b, I-70126 Bari, Italy

G. Eigen and B. Stugu
University of Bergen, Institute of Physics, N-5007 Bergen, Norway

D. N. Brown, L. T. Kerth, Yu. G. Kolomensky, M. J. Lee, and G. Lynch
Lawrence Berkeley National Laboratory and University of California, Berkeley, California 94720, USA

H. Koch and T. Schroeder
Ruhr Universität Bochum, Institut für Experimentalphysik 1, D-44780 Bochum, Germany

C. Hearty, T. S. Mattison, J. A. McKenna, and R. Y. So
University of British Columbia, Vancouver, British Columbia, Canada V6T 1Z1

A. Khan
Brunel University, Uxbridge, Middlesex UB8 3PH, United Kingdom

V. E. Blinov^{ac}, A. R. Buzykaev^a, V. P. Druzhinin^{ab}, V. B. Golubev^{ab}, E. A. Kravchenko^{ab}, A. P. Onuchin^{ac},
S. I. Serednyakov^{ab}, Yu. I. Skovpen^{ab}, E. P. Solodov^{ab}, K. Yu. Todyshev^{ab}, and A. N. Yushkov^a
*Budker Institute of Nuclear Physics SB RAS, Novosibirsk 630090^a,
Novosibirsk State University, Novosibirsk 630090^b,
Novosibirsk State Technical University, Novosibirsk 630092^c, Russia*

D. Kirkby, A. J. Lankford, and M. Mandelkern
University of California at Irvine, Irvine, California 92697, USA

B. Dey, J. W. Gary, O. Long, and G. M. Vitug
University of California at Riverside, Riverside, California 92521, USA

C. Campagnari, M. Franco Sevilla, T. M. Hong, D. Kovalskyi, J. D. Richman, and C. A. West
University of California at Santa Barbara, Santa Barbara, California 93106, USA

A. M. Eisner, W. S. Lockman, B. A. Schumm, and A. Seiden
University of California at Santa Cruz, Institute for Particle Physics, Santa Cruz, California 95064, USA

D. S. Chao, C. H. Cheng, B. Echenard, K. T. Flood, D. G. Hitlin, P. Ongmongkolkul, and F. C. Porter
California Institute of Technology, Pasadena, California 91125, USA

R. Andreassen, Z. Huard, B. T. Meadows, B. G. Pushpawela, M. D. Sokoloff, and L. Sun
University of Cincinnati, Cincinnati, Ohio 45221, USA

P. C. Bloom, W. T. Ford, A. Gaz, U. Nauenberg, J. G. Smith, and S. R. Wagner
University of Colorado, Boulder, Colorado 80309, USA

R. Ayad* and W. H. Toki

Colorado State University, Fort Collins, Colorado 80523, USA

B. Spaan

Technische Universität Dortmund, Fakultät Physik, D-44221 Dortmund, Germany

R. Schwierz

Technische Universität Dresden, Institut für Kern- und Teilchenphysik, D-01062 Dresden, Germany

D. Bernard and M. Verderi

Laboratoire Leprince-Ringuet, Ecole Polytechnique, CNRS/IN2P3, F-91128 Palaiseau, France

S. Playfer

University of Edinburgh, Edinburgh EH9 3JZ, United Kingdom

D. Bettoni^a, C. Bozzi^a, R. Calabrese^{ab}, G. Cibinetto^{ab}, E. Fioravanti^{ab},

I. Garzia^{ab}, E. Luppi^{ab}, L. Piemontese^a, and V. Santoro^a

INFN Sezione di Ferrara^a; Dipartimento di Fisica e Scienze della Terra, Università di Ferrara^b, I-44122 Ferrara, Italy

R. Baldini-Ferrolì, A. Calcaterra, R. de Sangro, G. Finocchiaro,

S. Martellotti, P. Patteri, I. M. Peruzzi,[†] M. Piccolo, M. Rama, and A. Zallo

INFN Laboratori Nazionali di Frascati, I-00044 Frascati, Italy

R. Contri^{ab}, E. Guido^{ab}, M. Lo Vetere^{ab}, M. R. Monge^{ab}, S. Passaggio^a, C. Patrignani^{ab}, and E. Robutti^a

INFN Sezione di Genova^a; Dipartimento di Fisica, Università di Genova^b, I-16146 Genova, Italy

B. Bhuyan and V. Prasad

Indian Institute of Technology Guwahati, Guwahati, Assam, 781 039, India

M. Morii

Harvard University, Cambridge, Massachusetts 02138, USA

A. Adametz and U. Uwer

Universität Heidelberg, Physikalisches Institut, D-69120 Heidelberg, Germany

H. M. Lacker

Humboldt-Universität zu Berlin, Institut für Physik, D-12489 Berlin, Germany

P. D. Dauncey

Imperial College London, London, SW7 2AZ, United Kingdom

U. Mallik

University of Iowa, Iowa City, Iowa 52242, USA

C. Chen, J. Cochran, W. T. Meyer, and S. Prell

Iowa State University, Ames, Iowa 50011-3160, USA

A. V. Gritsan

Johns Hopkins University, Baltimore, Maryland 21218, USA

N. Arnaud, M. Davier, D. Derkach, G. Grosdidier, F. Le Diberder,

A. M. Lutz, B. Malaescu,[‡] P. Roudeau, A. Stocchi, and G. Wormser

Laboratoire de l'Accélérateur Linéaire, IN2P3/CNRS et Université Paris-Sud 11,
Centre Scientifique d'Orsay, F-91898 Orsay Cedex, France

D. J. Lange and D. M. Wright

Lawrence Livermore National Laboratory, Livermore, California 94550, USA

J. P. Coleman, J. R. Fry, E. Gabathuler, D. E. Hutchcroft, D. J. Payne, and C. Touramanis

University of Liverpool, Liverpool L69 7ZE, United Kingdom

A. J. Bevan, F. Di Lodovico, and R. Sacco
Queen Mary, University of London, London, E1 4NS, United Kingdom

G. Cowan
University of London, Royal Holloway and Bedford New College, Egham, Surrey TW20 0EX, United Kingdom

J. Bougher, D. N. Brown, and C. L. Davis
University of Louisville, Louisville, Kentucky 40292, USA

A. G. Denig, M. Fritsch, W. Gradl, K. Griessinger, A. Hafner, E. Prencipe, and K. R. Schubert
Johannes Gutenberg-Universität Mainz, Institut für Kernphysik, D-55099 Mainz, Germany

R. J. Barlow[§] and G. D. Lafferty
University of Manchester, Manchester M13 9PL, United Kingdom

E. Behn, R. Cenci, B. Hamilton, A. Jawahery, and D. A. Roberts
University of Maryland, College Park, Maryland 20742, USA

R. Cowan, D. Dujmic, and G. Sciolla
Massachusetts Institute of Technology, Laboratory for Nuclear Science, Cambridge, Massachusetts 02139, USA

R. Cheaib, P. M. Patel,[¶] and S. H. Robertson
McGill University, Montréal, Québec, Canada H3A 2T8

P. Biassoni^{ab}, N. Neri^a, and F. Palombo^{ab}
INFN Sezione di Milano^a; Dipartimento di Fisica, Università di Milano^b, I-20133 Milano, Italy

L. Cremaldi, R. Godang,^{**} P. Sonnek, and D. J. Summers
University of Mississippi, University, Mississippi 38677, USA

M. Simard and P. Taras
Université de Montréal, Physique des Particules, Montréal, Québec, Canada H3C 3J7

G. De Nardo^{ab}, D. Monorchio^{ab}, G. Onorato^{ab}, and C. Sciacca^{ab}
*INFN Sezione di Napoli^a; Dipartimento di Scienze Fisiche,
Università di Napoli Federico II^b, I-80126 Napoli, Italy*

M. Martinelli and G. Raven
NIKHEF, National Institute for Nuclear Physics and High Energy Physics, NL-1009 DB Amsterdam, The Netherlands

C. P. Jessop and J. M. LoSecco
University of Notre Dame, Notre Dame, Indiana 46556, USA

K. Honscheid and R. Kass
Ohio State University, Columbus, Ohio 43210, USA

J. Brau, R. Frey, N. B. Sinev, D. Strom, and E. Torrence
University of Oregon, Eugene, Oregon 97403, USA

E. Feltresi^{ab}, M. Margoni^{ab}, M. Morandin^a, M. Posocco^a, M. Rotondo^a, G. Simi^a, F. Simonetto^{ab}, and R. Stroili^{ab}
INFN Sezione di Padova^a; Dipartimento di Fisica, Università di Padova^b, I-35131 Padova, Italy

S. Akar, E. Ben-Haim, M. Bomben, G. R. Bonneaud, H. Briand,
G. Calderini, J. Chauveau, Ph. Leruste, G. Marchiori, J. Ocariz, and S. Sitt
*Laboratoire de Physique Nucléaire et de Hautes Energies,
IN2P3/CNRS, Université Pierre et Marie Curie-Paris6,*

Université Denis Diderot-Paris7, F-75252 Paris, France

M. Biasini^{ab}, E. Manoni^a, S. Pacetti^{ab}, and A. Rossi^a
INFN Sezione di Perugia^a; Dipartimento di Fisica, Università di Perugia^b, I-06123 Perugia, Italy

C. Angelini^{ab}, G. Batignani^{ab}, S. Bettarini^{ab}, M. Carpinelli^{ab,††}, G. Casarosa^{ab}, A. Cervelli^{ab}, F. Forti^{ab},
 M. A. Giorgi^{ab}, A. Lusiani^{ac}, B. Oberhof^{ab}, E. Paoloni^{ab}, A. Perez^a, G. Rizzo^{ab}, and J. J. Walsh^a
INFN Sezione di Pisa^a; Dipartimento di Fisica, Università di Pisa^b; Scuola Normale Superiore di Pisa^c, I-56127 Pisa, Italy

D. Lopes Pegna, J. Olsen, and A. J. S. Smith
Princeton University, Princeton, New Jersey 08544, USA

R. Faccini^{ab}, F. Ferrarotto^a, F. Ferroni^{ab}, M. Gaspero^{ab}, L. Li Gioi^a, and G. Piredda^a
*INFN Sezione di Roma^a; Dipartimento di Fisica,
 Università di Roma La Sapienza^b, I-00185 Roma, Italy*

C. Büniger, O. Grünberg, T. Hartmann, T. Leddig, C. Voß, and R. Waldi
Universität Rostock, D-18051 Rostock, Germany

T. Adye, E. O. Olaiya, and F. F. Wilson
Rutherford Appleton Laboratory, Chilton, Didcot, Oxon, OX11 0QX, United Kingdom

S. Emery, G. Hamel de Monchenault, G. Vasseur, and Ch. Yèche
CEA, Irfu, SPP, Centre de Saclay, F-91191 Gif-sur-Yvette, France

F. Anulli,^{‡‡} D. Aston, D. J. Bard, J. F. Benitez, C. Cartaro, M. R. Convery, J. Dorfan, G. P. Dubois-Felsmann,
 W. Dunwoodie, M. Ebert, R. C. Field, B. G. Fulsom, A. M. Gabareen, M. T. Graham, C. Hast,
 W. R. Innes, P. Kim, M. L. Kocian, D. W. G. S. Leith, P. Lewis, D. Lindemann, B. Lindquist, S. Luitz,
 V. Luth, H. L. Lynch, D. B. MacFarlane, D. R. Muller, H. Neal, S. Nelson, M. Perl, T. Pulliam,
 B. N. Ratcliff, A. Roodman, A. A. Salnikov, R. H. Schindler, A. Snyder, D. Su, M. K. Sullivan, J. Va'vra,
 A. P. Wagner, W. F. Wang, W. J. Wisniewski, M. Wittgen, D. H. Wright, H. W. Wulsin, and V. Ziegler
SLAC National Accelerator Laboratory, Stanford, California 94309 USA

W. Park, M. V. Purohit, R. M. White,^{§§} and J. R. Wilson
University of South Carolina, Columbia, South Carolina 29208, USA

A. Randle-Conde and S. J. Sekula
Southern Methodist University, Dallas, Texas 75275, USA

M. Bellis, P. R. Burchat, T. S. Miyashita, and E. M. T. Puccio
Stanford University, Stanford, California 94305-4060, USA

M. S. Alam and J. A. Ernst
State University of New York, Albany, New York 12222, USA

R. Gorodeisky, N. Guttman, D. R. Peimer, and A. Soffer
Tel Aviv University, School of Physics and Astronomy, Tel Aviv, 69978, Israel

S. M. Spanier
University of Tennessee, Knoxville, Tennessee 37996, USA

J. L. Ritchie, A. M. Ruland, R. F. Schwitters, and B. C. Wray
University of Texas at Austin, Austin, Texas 78712, USA

J. M. Izen and X. C. Lou
University of Texas at Dallas, Richardson, Texas 75083, USA

F. Bianchi^{ab}, F. De Mori^{ab}, A. Filippi^a, D. Gamba^{ab}, and S. Zambito^{ab}

INFN Sezione di Torino^a; Dipartimento di Fisica, Università di Torino^b, I-10125 Torino, Italy

L. Lancieri^{ab} and L. Vitale^{ab}

INFN Sezione di Trieste^a; Dipartimento di Fisica, Università di Trieste^b, I-34127 Trieste, Italy

F. Martinez-Vidal, A. Oyanguren, and P. Villanueva-Perez
IFIC, Universitat de Valencia-CSIC, E-46071 Valencia, Spain

H. Ahmed, J. Albert, Sw. Banerjee, F. U. Bernlochner, H. H. F. Choi, G. J. King, R. Kowalewski,
M. J. Lewczuk, T. Lueck, I. M. Nugent, J. M. Roney, R. J. Sobie, and N. Tasneem
University of Victoria, Victoria, British Columbia, Canada V8W 3P6

T. J. Gershon, P. F. Harrison, and T. E. Latham
Department of Physics, University of Warwick, Coventry CV4 7AL, United Kingdom

H. R. Band, S. Dasu, Y. Pan, R. Prepost, and S. L. Wu
University of Wisconsin, Madison, Wisconsin 53706, USA

The $e^+e^- \rightarrow p\bar{p}$ cross section and the proton magnetic form factor have been measured in the center-of-mass energy range from 3.0 to 6.5 GeV using the initial-state-radiation technique with an undetected photon. This is the first measurement of the form factor at energies higher than 4.5 GeV. The analysis is based on 469 fb^{-1} of integrated luminosity collected with the BABAR detector at the PEP-II collider at e^+e^- center-of-mass energies near 10.6 GeV. The branching fractions for the decays $J/\psi \rightarrow p\bar{p}$ and $\psi(2S) \rightarrow p\bar{p}$ have also been measured.

PACS numbers: 13.66.Bc, 14.20.Dh, 13.40.Gp, 13.25.Gv

I. INTRODUCTION

In this paper we analyze the initial-state-radiation (ISR) process $e^+e^- \rightarrow p\bar{p}\gamma$ represented by Fig. 1. This analysis is a continuation of our previous studies [1, 2], where the ISR technique was used to measure the cross section of the nonradiative process $e^+e^- \rightarrow p\bar{p}$ over the center-of-mass (c.m.) energy range from $p\bar{p}$ threshold, $2m_p c^2 = 1.88 \text{ GeV}$, up to 4.5 GeV. In Refs. [1, 2] it is required that the ISR photon be detected (large-angle ISR). In this paper, we analyze events in which the ISR photon is emitted along the e^+e^- collision axis (small-angle ISR) and is therefore not detected. This allows us to increase the detection efficiency for ISR events with $p\bar{p}$ invariant mass above 3.2 GeV/ c^2 , to select $p\bar{p}\gamma$ events with lower background, and, therefore, to extend the en-

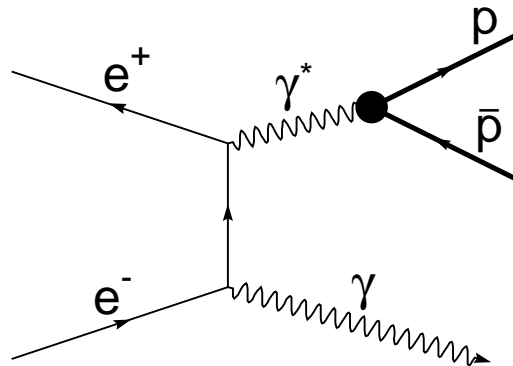


FIG. 1: The Feynman diagram for the ISR process $e^+e^- \rightarrow p\bar{p}\gamma$.

*Now at the University of Tabuk, Tabuk 71491, Saudi Arabia

†Also with Università di Perugia, Dipartimento di Fisica, Perugia, Italy

‡Now at Laboratoire de Physique Nucléaire et de Hautes Energies, IN2P3/CNRS, Paris, France

§Now at the University of Huddersfield, Huddersfield HD1 3DH, UK

¶Deceased

**Now at University of South Alabama, Mobile, Alabama 36688, USA

††Also with Università di Sassari, Sassari, Italy

‡‡Also with INFN Sezione di Roma, Roma, Italy

§§Now at Universidad Técnica Federico Santa María, Valparaiso, Chile 2390123

ergy range for measurement of the $e^+e^- \rightarrow p\bar{p}$ cross section. A discussion of the difference between the large- and small-angle ISR techniques is given in Ref. [3].

The Born cross section for the ISR process integrated over the nucleon momenta and the photon polar angle is given by

$$\frac{d\sigma_{e^+e^- \rightarrow p\bar{p}\gamma}(M_{p\bar{p}})}{dM_{p\bar{p}}} = \frac{2M_{p\bar{p}}}{s} W(s, x) \sigma_{p\bar{p}}(M_{p\bar{p}}), \quad (1)$$

where $M_{p\bar{p}}$ is the $p\bar{p}$ invariant mass, s is the e^+e^- c.m. energy squared, $x \equiv E_\gamma^*/\sqrt{s} = 1 - M_{p\bar{p}}^2/s$, and E_γ^* is the ISR

photon energy in the e^+e^- c.m. frame¹. The function [3]

$$W(s, x) = \frac{\alpha}{\pi x} \left(\ln \frac{s}{m_e^2} - 1 \right) (2 - 2x + x^2) \quad (2)$$

specifies the probability of ISR photon emission, where α is the fine structure constant and m_e is the electron mass. Equations (1) and (2) describe ISR processes at lowest QED order. To calculate the function $W(x)$ more precisely, taking into account higher-order diagrams involving loops and extra photon emission, we make use of the analytic techniques described in Refs. [4–6] and the Monte Carlo (MC) generator of ISR events, Phokhara [7].

The cross section for $e^+e^- \rightarrow p\bar{p}$ is given by

$$\sigma_{p\bar{p}}(M_{p\bar{p}}) = \frac{4\pi\alpha^2\beta C}{3M_{p\bar{p}}^2} \left[|G_M(M_{p\bar{p}})|^2 + \frac{2m_p^2}{M_{p\bar{p}}^2} |G_E(M_{p\bar{p}})|^2 \right], \quad (3)$$

where $\beta = \sqrt{1 - 4m_p^2/M_{p\bar{p}}^2}$, $C = y/(1 - e^{-y})$ is the Coulomb correction factor [8], and $y = \pi\alpha(1 + \beta^2)/\beta$. The Coulomb factor makes the cross section nonzero at threshold. The cross section depends on the magnetic (G_M) and electric (G_E) form factors. At large $p\bar{p}$ invariant masses the second term in Eq. (3) is suppressed as $2m_p^2/M_{p\bar{p}}^2$, and therefore the measured total cross section is not very sensitive to the value of the electric form factor. The value of the magnetic form factor can be extracted from the measured cross section with relatively small model uncertainty using, for example, the assumption that $|G_M| = |G_E|$ [9–11].

The existing experimental data on $|G_M(M_{p\bar{p}})|$ at high $p\bar{p}$ invariant masses were obtained in e^+e^- [2, 9–11] and $p\bar{p}$ annihilation [12, 13]. At energies higher than 3 GeV the value of the magnetic form factor decreases rapidly with increasing energy. The energy dependence measured in Refs. [2, 10, 12, 13] agrees with the dependence $\alpha_s^2(M_{p\bar{p}}^2)/M_{p\bar{p}}^4$ predicted by QCD for the asymptotic proton form factor [14]. However, the two precision measurements of Ref. [11] based on CLEO data indicate that the decrease of the form factor at energies near 4 GeV is somewhat slower.

In this work we improve the accuracy of our measurements of the $e^+e^- \rightarrow p\bar{p}$ cross section and of the proton magnetic form factor for $p\bar{p}$ invariant masses greater than 3 GeV/ c^2 , and extend the range of measurement up to 6.5 GeV/ c^2 .

II. THE BABAR DETECTOR, DATA AND SIMULATED SAMPLES

We analyse a data sample corresponding to an integrated luminosity of 469 fb⁻¹ [15] recorded with the

BABAR detector [16] at the SLAC PEP-II asymmetric-energy (9-GeV e^- and 3.1-GeV e^+) collider. About 90% of the data were collected at an e^+e^- c.m. energy of 10.58 GeV (the $\Upsilon(4S)$ mass), and the remainder at 10.54 GeV.

Charged-particle tracking is provided by a five-layer silicon vertex tracker (SVT) and a 40-layer drift chamber (DCH), operating in the 1.5 T magnetic field of a superconducting solenoid. The transverse momentum resolution is 0.47% at 1 GeV/ c . The position and energy of a photon-produced cluster are measured with a CsI(Tl) electromagnetic calorimeter. Charged-particle identification (PID) is provided by specific ionization measurements in the SVT and DCH, and by an internally reflecting ring-imaging Cherenkov detector. Muons are identified in the solenoid's instrumented flux return.

The events of the process under study and the background processes $e^+e^- \rightarrow \pi^+\pi^-\gamma$, $K^+K^-\gamma$, and $\mu^+\mu^-\gamma$ are simulated with the Phokhara [7] event generator, which takes into account next-to-leading-order radiative corrections. To estimate the model uncertainty of our measurement, the simulation for the signal process is performed under two form-factor assumptions, namely $|G_M| = |G_E|$ and $|G_E| = 0$. To obtain realistic estimates of pion and kaon backgrounds, the experimental values of the pion and kaon electromagnetic form factors measured by the CLEO Collaboration at $\sqrt{s} = 3.67$ GeV [10] are used in the event generator. The invariant-mass dependence of the form factors is assumed to be $1/m^2$, according to the QCD prediction for the asymptotic behavior of the form factors [17]. The $e^+e^- \rightarrow e^+e^-\gamma$ process is simulated with the BHWIDE [18] event generator.

Background from the two-photon process $e^+e^- \rightarrow e^+e^-p\bar{p}$ is simulated with the GamGam event generator [19]. In addition, possible background contributions from $e^+e^- \rightarrow q\bar{q}$, where q represents a u , d or s quark, are simulated with the JETSET [20] event generator. Since JETSET also generates ISR events, it can be used to study background from ISR processes with extra π^0 's, such as $e^+e^- \rightarrow p\bar{p}\pi^0\gamma$, $p\bar{p}\pi^0\pi^0\gamma$, etc. The most important non-ISR background process, $e^+e^- \rightarrow p\bar{p}\pi^0$, is simulated separately [1].

The detector response is simulated using the Geant4 [21] package. The simulation takes into account the variations in the detector and beam-background conditions over the running period of the experiment.

III. EVENT SELECTION

We select events with two charged-particle tracks with opposite charge originating from the interaction region. Each track must have transverse momentum greater than 0.1 GeV/ c , be in the polar angle range $25.8^\circ < \theta < 137.5^\circ$, and be identified as a proton or antiproton. The pair of proton and antiproton candidates is fit to a common vertex with a beam-spot constraint, and the χ^2 probability for this fit is required to exceed 0.1%.

¹ Throughout this paper, the asterisk denotes quantities in the e^+e^- c.m. frame; all other variables are given in the laboratory frame.

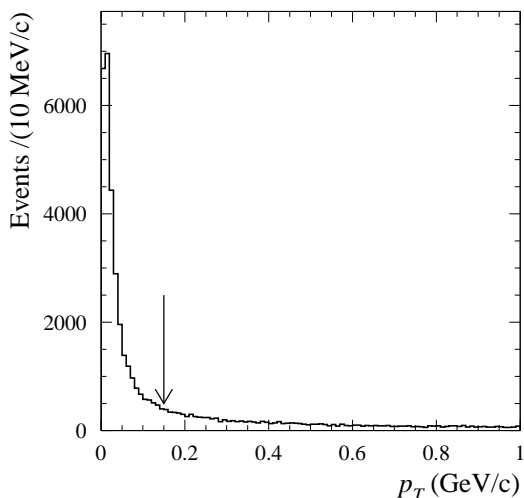


FIG. 2: The distribution of the $p\bar{p}$ transverse momentum for simulated $e^+e^- \rightarrow p\bar{p}\gamma$ events. The arrow indicates $p_T = 0.150$ GeV/ c .

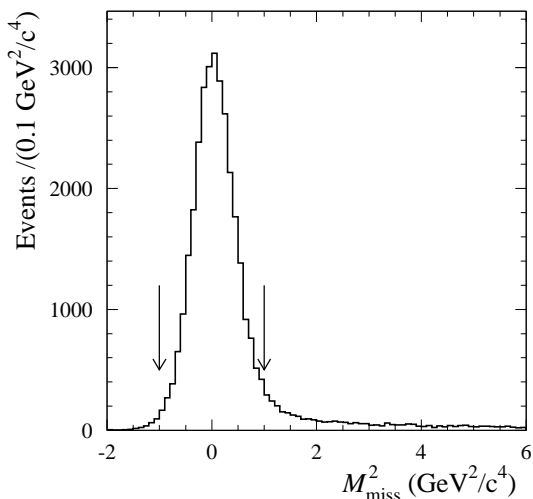


FIG. 3: The M_{miss}^2 distribution for simulated $e^+e^- \rightarrow p\bar{p}\gamma$ events, where M_{miss}^2 is the missing-mass-squared recoiling against the $p\bar{p}$ system. The arrows indicate $|M_{\text{miss}}^2| = 1$ GeV $^2/c^4$.

The final event selection is based on two variables: the $p\bar{p}$ transverse momentum (p_T) and the missing-mass-squared (M_{miss}^2) recoiling against the $p\bar{p}$ system. The p_T distribution for simulated $e^+e^- \rightarrow p\bar{p}\gamma$ events is shown in Fig. 2. The peak near zero corresponds to ISR photons emitted along the collision axis, while the long tail is due to photons emitted at large angles. We apply the condition $p_T < 0.15$ GeV/ c , which removes large-angle ISR events, and strongly suppresses background from the process $e^+e^- \rightarrow p\bar{p}\pi^0$ and from ISR processes with extra π^0 's. The process $e^+e^- \rightarrow p\bar{p}\pi^0$ was the dominant

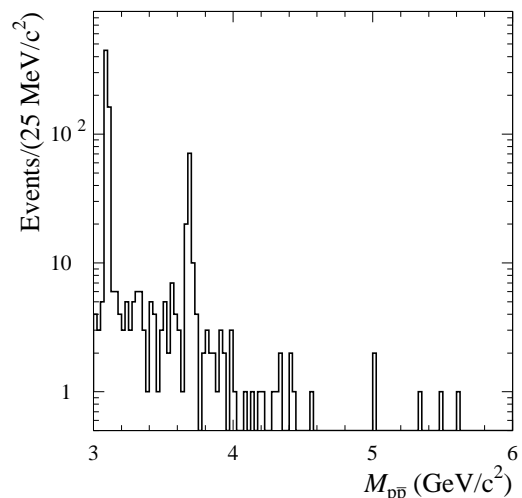


FIG. 4: The $p\bar{p}$ invariant-mass spectrum for selected data $p\bar{p}\gamma$ candidates.

background source at large invariant masses in our previous studies of the $e^+e^- \rightarrow p\bar{p}\gamma$ process with large-angle ISR [1, 2].

In the e^+e^- c.m. frame protons with low $p\bar{p}$ invariant masses are produced in a narrow cone around the vector opposite to the ISR photon direction. Due to limited detector acceptance, the low-mass region cannot be studied with small-angle ISR. A $p\bar{p}$ pair with $p_T < 0.15$ GeV/ c is detected in *BABAR* when its invariant mass is larger than 3.0 (4.5) GeV/ c^2 for an ISR photon emitted along the electron (positron) beam direction. The corresponding average proton or antiproton momentum in the laboratory frame is about 2 (5) GeV/ c . The difference between the two photon directions arises from the energy asymmetry of the e^+e^- collisions at PEP-II. Since particle misidentification probability strongly increases at large momentum, we reject events with the ISR photon emitted along the positron beam. This condition decreases the detection efficiency by about 20% for signal events with invariant masses above 5 GeV/ c^2 .

The missing-mass-squared distribution for simulated $e^+e^- \rightarrow p\bar{p}\gamma$ events is shown in Fig. 3. We select events with $|M_{\text{miss}}^2| < 1$ GeV $^2/c^4$. This condition suppresses background from two-photon and ISR events, which have large positive M_{miss}^2 , and background from $e^+e^- \rightarrow e^+e^-\gamma$, $\mu^+\mu^-\gamma$ events, which have negative M_{miss}^2 . Sideband regions in M_{miss}^2 and in p_T for ISR background are used to estimate remaining background contributions from these sources.

The $p\bar{p}$ invariant-mass spectrum for the selected data candidates is shown in Fig. 4. The total number of selected events is 845. About 80% of selected events originate from $J/\psi \rightarrow p\bar{p}$ and $\psi(2S) \rightarrow p\bar{p}$ decays. We do not observe events with invariant mass above 6 GeV/ c^2 .

IV. BACKGROUND ESTIMATION AND SUBTRACTION

The processes $e^+e^- \rightarrow \pi^+\pi^-\gamma$, $K^+K^-\gamma$, $\mu^+\mu^-\gamma$, and $e^+e^- \rightarrow e^+e^-\gamma$ in which the charged particles are misidentified as protons, are potential sources of background in the sample of selected data events. In addition, the two-photon process $e^+e^- \rightarrow e^+e^-p\bar{p}$, and processes with protons and neutral particles in the final state, such as $e^+e^- \rightarrow p\bar{p}\pi^0$ and $e^+e^- \rightarrow p\bar{p}\pi^0\gamma$, may yield background contributions.

A. Background from $e^+e^- \rightarrow \pi^+\pi^-\gamma$, $e^+e^- \rightarrow K^+K^-\gamma$, $e^+e^- \rightarrow \mu^+\mu^-\gamma$, and $e^+e^- \rightarrow e^+e^-\gamma$

In Ref. [2] it was shown that the *BABAR* MC simulation reproduces reasonably well the probability for a pion or a kaon to be identified as a proton. Consequently, the simulation is used to estimate the $e^+e^- \rightarrow \pi^+\pi^-\gamma$ and $e^+e^- \rightarrow K^+K^-\gamma$ background contributions in the present analysis. No events satisfying the selection criteria for $p\bar{p}\gamma$ are observed in the $\pi^+\pi^-\gamma$ and $K^+K^-\gamma$ MC samples. Since these MC samples exceed those expected for pion and kaon events in data by about an order of magnitude, we conclude that these background sources can be neglected.

To estimate possible electron and muon background a method based on the difference in the M_{miss}^2 distributions for signal and background events is used. For $e^+e^- \rightarrow \mu^+\mu^-\gamma$ events the ratio of the number of events with $|M_{\text{miss}}^2| < 1 \text{ GeV}^2/c^4$ to the number with $M_{\text{miss}}^2 < -1 \text{ GeV}^2/c^4$ varies from 0.03 to about 0.1 in the $M_{p\bar{p}}$ range of interest. Smaller values are expected for $e^+e^- \rightarrow e^+e^-\gamma$ events. In data we observe 15 events with $M_{\text{miss}}^2 < -1 \text{ GeV}^2/c^4$, of which 6 events are expected to originate from signal (of these, 5 are from $J/\psi \rightarrow p\bar{p}$ and $\psi(2S) \rightarrow p\bar{p}$ decays). From the ratio values given above, we estimate that muon and electron background in our selected event sample does not exceed 1 event. The estimated background contributions for different invariant-mass intervals are listed in Table I.

B. Two-photon background

Figure 5 shows the M_{miss}^2 distribution for data events selected using all the criteria described in Sec. III except $|M_{\text{miss}}^2| < 1 \text{ GeV}^2/c^4$. Events with large recoil mass arise from the two-photon process $e^+e^- \rightarrow e^+e^-\gamma^*\gamma^* \rightarrow e^+e^-p\bar{p}$. The two-photon background in the region $|M_{\text{miss}}^2| < 1 \text{ GeV}^2/c^4$ is estimated from the number of data events with $M_{\text{miss}}^2 > d$ using the scale factor $R_{\gamma\gamma} = N_{\gamma\gamma}(|M_{\text{miss}}^2| < 1)/N_{\gamma\gamma}(M_{\text{miss}}^2 > d)$ obtained from the $e^+e^- \rightarrow e^+e^-p\bar{p}$ simulation. Since the M_{miss}^2 distribution for two-photon events changes with $p\bar{p}$ invariant mass, the parameter d is changed from 40 GeV^2/c^4 for the invariant-mass interval 3.0–3.2 GeV/c^2

TABLE I: The number of selected $p\bar{p}\gamma$ candidates (N_{data}) and the estimated numbers of background events from the processes $e^+e^- \rightarrow \mu^+\mu^-\gamma$ and $e^+e^- \rightarrow e^+e^-\gamma$ ($N_{\ell\ell\gamma}$), $e^+e^- \rightarrow e^+e^-p\bar{p}$ ($N_{2\gamma}$), and the ISR processes with extra neutral particle(s), such as $e^+e^- \rightarrow p\bar{p}\pi^0\gamma$, $p\bar{p}2\pi^0\gamma$ ($N_{\text{bkg}}^{\text{ISR}}$). In the invariant-mass intervals 3.0–3.2 GeV/c^2 and 3.6–3.8 GeV/c^2 the contribution of the $J/\psi \rightarrow p\bar{p}$ and $\psi(2S) \rightarrow p\bar{p}$ decays are subtracted (see Sec. VI), with related statistical uncertainties reported.

$M_{p\bar{p}}$ (GeV/c^2)	N_{data}	$N_{\ell\ell\gamma}$	$N_{2\gamma}$	$N_{\text{bkg}}^{\text{ISR}}$
3.0–3.2	35 ± 7	< 0.1	0.5 ± 0.4	1.5 ± 0.6
3.2–3.4	32	< 0.1	0.5 ± 0.3	1.3 ± 0.6
3.4–3.6	31	< 0.1	0.15 ± 0.10	0.7 ± 0.5
3.6–3.8	17 ± 5	< 0.1	0.20 ± 0.10	0.0 ± 0.2
3.8–4.0	16	< 0.1	0.10 ± 0.04	0.7 ± 0.4
4.0–4.5	12	< 0.1	0.10 ± 0.03	0.7 ± 0.4
4.5–5.5	5	< 0.3	0.05 ± 0.02	1.0 ± 0.5
5.5–6.5	1	< 0.3	< 0.01	0.4 ± 0.3

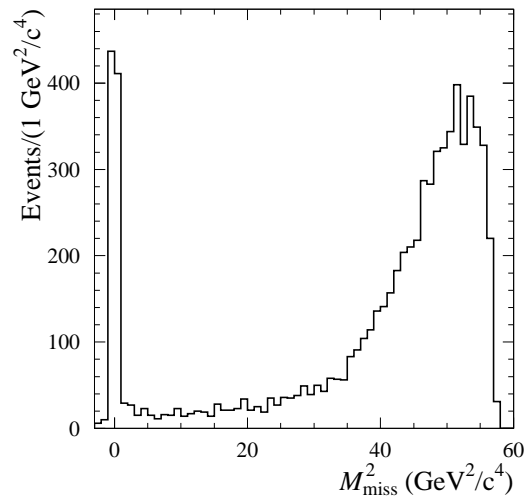


FIG. 5: The M_{miss}^2 distribution for data events selected using all the criteria described in Sec. III except $|M_{\text{miss}}^2| < 1 \text{ GeV}^2/c^4$.

to 15 GeV^2/c^4 for the interval 5.5–6.5 GeV/c^2 . To determine a realistic value of the scale factor, the simulated events are reweighted according to the proton angular distribution observed in data. The value of the scale factor is found to increase from 5×10^{-4} in the 3.0–3.2 GeV/c^2 interval to 2×10^{-2} in the 5.5–6.5 GeV/c^2 interval. Fortunately, the number of observed two-photon events decreases significantly over this same range. The estimated number of two-photon background events for each invariant-mass interval is listed in Table I. The background is found to be small, at the level of 1%.

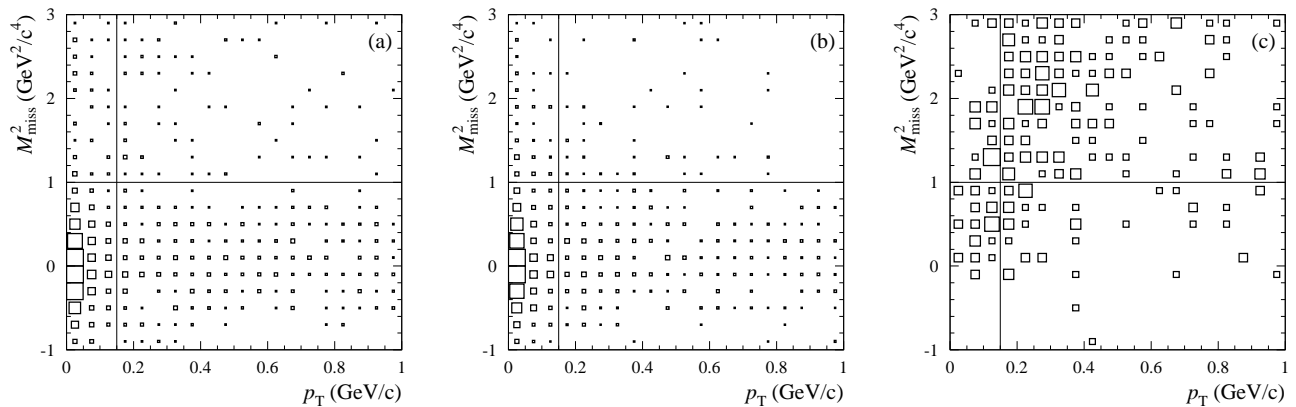


FIG. 6: The distributions of M_{miss}^2 versus p_T (a) for data events with $M_{p\bar{p}} > 3.2 \text{ GeV}/c^2$, (b) for simulated signal events, and (c) for simulated ISR background events.

C. ISR background

To estimate background from ISR processes with at least one extra neutral particle, such as $e^+e^- \rightarrow p\bar{p}\pi^0\gamma$, $e^+e^- \rightarrow p\bar{p}\eta\gamma$, $e^+e^- \rightarrow p\bar{p}\pi^0\pi^0\gamma$, etc., we use differences in the p_T and M_{miss}^2 distributions for signal and background events. Figure 6 shows the two-dimensional distributions of M_{miss}^2 versus p_T for data events with $M_{p\bar{p}} > 3.2 \text{ GeV}/c^2$, and for simulated signal and ISR background events. The ISR background is simulated using the JETSET event generator. It should be noted that most of the background events (about 90%) shown in Fig. 6 arise from $e^+e^- \rightarrow p\bar{p}\pi^0\gamma$. The lines in Fig. 6 indicate the boundaries of the signal region (bottom left rectangle) and of the sideband region (top right rectangle). The number of data events in the sideband (N_2) is used to estimate the number of background events in the signal region by using

$$N_{\text{bkg}}^{\text{ISR}} = \frac{N_2 - \beta_{\text{sig}}N_1}{\beta_{\text{bkg}} - \beta_{\text{sig}}}, \quad (4)$$

where N_1 is the number of data events in the signal region, and β_{sig} and β_{bkg} are the N_2/N_1 ratios for the signal and background, respectively. These ratios are determined from MC simulation to be $\beta_{\text{sig}} = 0.043 \pm 0.002$ and $\beta_{\text{bkg}} = 5 \pm 1$. Both coefficients are found to be practically independent of $p\bar{p}$ invariant mass. The estimated numbers of ISR background events for different invariant-mass regions are listed in Table I. This is the main source of background for the process under study.

The background from the process $e^+e^- \rightarrow p\bar{p}\pi^0$, which was the dominant background source in our previous large-angle studies [1, 2], is found to be negligible in the data sample selected with the criteria for small-angle ISR events.

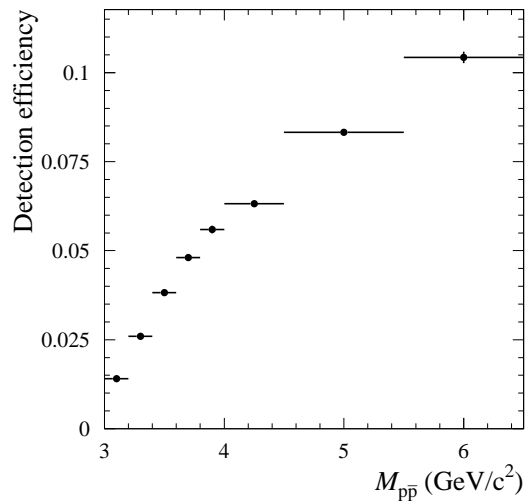


FIG. 7: The $p\bar{p}$ invariant-mass dependence of the detection efficiency obtained from MC simulation in the model with $|G_E| = |G_M|$.

V. DETECTION EFFICIENCY

The detection efficiency determined using MC simulation is shown in Fig. 7 as a function of $p\bar{p}$ invariant mass. The efficiency is calculated under the assumption that $|G_E| = |G_M|$. To study the model dependence of the detection efficiency, we analyze a sample of MC events produced using a model with $G_E = 0$. The ratio of the efficiencies obtained in the two models is shown in Fig. 8. The deviation of this ratio from unity is taken as an estimate of the model uncertainty on the detection efficiency.

The efficiency determined from MC simulation (ε_{MC}) must be corrected to account for data-MC simulation dif-

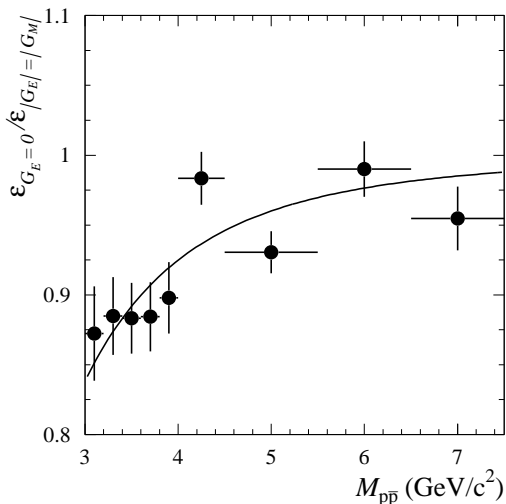


FIG. 8: The ratio of the detection efficiencies obtained from MC simulation using $G_E = 0$ and using $|G_E| = |G_M|$. The solid curve is drawn to guide the eye.

TABLE II: The values of the efficiency corrections, δ_i .

Source	δ_i (%)
Track reconstruction	0.0 ± 0.5
Nuclear interaction	1.1 ± 0.4
PID	-1.9 ± 2.0
Conditions on p_T and M_{miss}^2	4.3 ± 2.6
Total	3.5 ± 3.3

ferences in detector response according to

$$\varepsilon = \varepsilon_{MC} \prod (1 + \delta_i), \quad (5)$$

where the δ_i are the efficiency corrections listed in Table II. The corrections for data-MC simulation differences in track reconstruction, nuclear interaction, and PID were estimated in our previous publications [1, 2]. Systematic effects on p_T and M_{miss}^2 may bias the estimated efficiency through the selection criteria. This is studied using $e^+e^- \rightarrow J/\psi\gamma \rightarrow p\bar{p}\gamma$ events. In Sec. VI the number of J/ψ events is determined with the requirements $p_T < 1$ GeV/c and $-2 < M_{\text{miss}}^2 < 3$ GeV²/c⁴, which are significantly looser than our standard criteria. The double data-MC simulation ratio of the numbers of J/ψ events selected with the standard and looser criteria, 1.043 ± 0.026 , is used to estimate the efficiency correction. The corrected values of the detection efficiency are listed in Table III.

VI. J/ψ AND $\psi(2S)$ DECAYS INTO $p\bar{p}$

The $p\bar{p}$ invariant-mass spectra for selected events in the J/ψ and $\psi(2S)$ invariant-mass regions are shown in

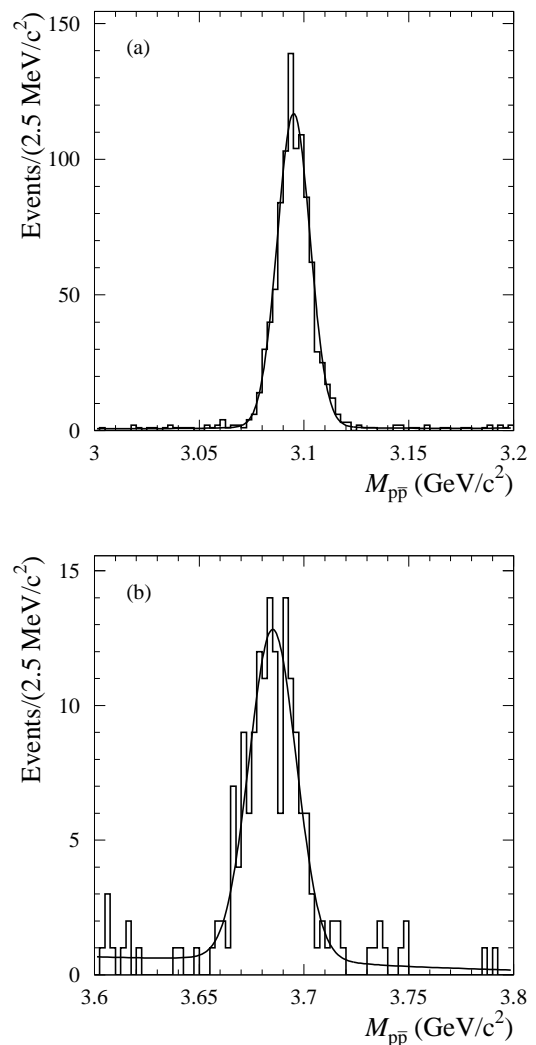


FIG. 9: The $p\bar{p}$ invariant-mass spectrum in the invariant-mass region near (a) the J/ψ , and (b) the $\psi(2S)$. The curves show the results of the fits described in the text.

Fig. 9. The events are selected by requiring $p_T < 1$ GeV/c and $-2 < M_{\text{miss}}^2 < 3$ GeV²/c⁴. To determine the number of resonance events, both spectra are fitted using the sum of a probability density function (PDF) for resonance events and a linear background function. The resonance PDF is a Breit-Wigner function convolved with a double-Gaussian function describing detector resolution. The parameters of the resolution function are determined from simulation. To account for possible differences in detector response between data and simulation, the simulated resolution function is modified by allowing an additional σ_G to be added in quadrature to both σ 's of the double-Gaussian function and by introducing the possibility of an invariant-mass shift. The free parameters in the fit to the J/ψ invariant-mass region are the number of resonance events, the total number of nonresonant background events, the slope of the background function,

σ_G , and the mass shift parameter. In the $\psi(2S)$ fit, σ_G is fixed to the value obtained from the J/ψ fit. The result of the fit for the J/ψ region is shown by the solid curve in Fig. 9(a), and the corresponding signal yield is 918 ± 31 events. Similarly, the solid curve in Fig. 9(b) shows the fit result for the $\psi(2S)$ region, with signal yield of 142 ± 13 events.

The detection efficiency is estimated from MC simulation. The event generator uses the experimental data on the polar-angle distribution of the proton in $\psi \rightarrow p\bar{p}$ decay. The distribution is described by the function $1 + a \cos^2 \vartheta$ with $a = 0.595 \pm 0.019$ for J/ψ [22] and 0.72 ± 0.13 for $\psi(2S)$ [23, 24]. The model error on the detection efficiency due to the uncertainty of a is estimated to be 1.5% for the J/ψ and 5% for the $\psi(2S)$. The efficiencies (ε_{MC}) are found to be $(2.20 \pm 0.02)\%$ for the J/ψ and $(6.86 \pm 0.04)\%$ for the $\psi(2S)$. The data-MC simulation differences discussed earlier are used to correct the above efficiency values by $(-0.8 \pm 2.1)\%$ (Table II, corrections 1–3).

The value of the cross section for the production of the J/ψ or $\psi(2S)$ followed by its decay to $p\bar{p}$ is given by $N/(\varepsilon L)$, where N is the number of signal events extracted in the fit shown in Fig. 9(a) or Fig. 9(b), ε is the relevant detection efficiency, and L is the nominal integrated luminosity. The cross section values obtained in this way are $(89.5 \pm 3.0 \pm 2.8)$ fb and $(4.45 \pm 0.41 \pm 0.25)$ fb for the J/ψ and $\psi(2S)$, respectively, where the first error is statistical and the second systematic.

These values correspond to the integral of the right-hand side of Eq. (1) over the resonance lineshape, *i.e.* for resonance R

$$\sigma_{\text{meas}} = \int \frac{2m}{s} W(s, x) \sigma_R(m) dm, \quad (6)$$

where m runs over the resonance region. For a narrow resonance

$$\sigma_{\text{meas}} = W(s, x_R) \frac{12\pi^2 \Gamma(R \rightarrow e^+e^-) \mathcal{B}(R \rightarrow p\bar{p})}{s m_R} \quad (7)$$

is a very good approximation, where $x_R = 1 - m_R^2/s$, and m_R is the resonance mass.

From the measured values of the cross section we thus obtain:

$$\begin{aligned} \Gamma(J/\psi \rightarrow e^+e^-) \mathcal{B}(J/\psi \rightarrow p\bar{p}) &= \\ &= (12.9 \pm 0.4 \pm 0.4) \text{ eV}, \\ \Gamma(\psi(2S) \rightarrow e^+e^-) \mathcal{B}(\psi(2S) \rightarrow p\bar{p}) &= \\ &= (0.74 \pm 0.07 \pm 0.04) \text{ eV}. \end{aligned} \quad (8)$$

The systematic error includes the uncertainties of the detection efficiency, the integrated luminosity (1%), and the theoretical uncertainty on the production cross section (1%).

Using the nominal values of the e^+e^- widths [25], the $\psi \rightarrow p\bar{p}$ branching fractions are calculated to be

$$\begin{aligned} \mathcal{B}(J/\psi \rightarrow p\bar{p}) &= (2.33 \pm 0.08 \pm 0.09) \times 10^{-3}, \\ \mathcal{B}(\psi(2S) \rightarrow p\bar{p}) &= (3.14 \pm 0.28 \pm 0.18) \times 10^{-4}. \end{aligned} \quad (9)$$

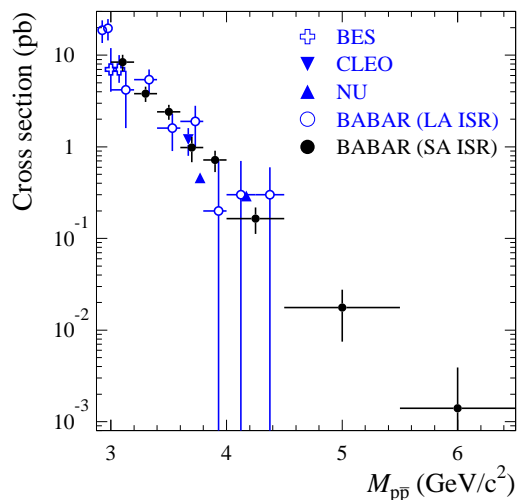


FIG. 10: The $e^+e^- \rightarrow p\bar{p}$ cross section measured in this analysis [BABAR (SA ISR)] and in other experiments: BES [9], CLEO [10], NU [11], and BABAR (LA ISR) [2].

These values are in agreement with the corresponding nominal values [25], $(2.17 \pm 0.07) \times 10^{-3}$ and $(2.76 \pm 0.12) \times 10^{-4}$, and with the recent BESIII measurement [22] $\mathcal{B}(J/\psi \rightarrow p\bar{p}) = (2.11 \pm 0.03) \times 10^{-3}$.

VII. THE $e^+e^- \rightarrow p\bar{p}$ CROSS SECTION AND THE PROTON FORM FACTOR

The cross section for $e^+e^- \rightarrow p\bar{p}$ in each $p\bar{p}$ invariant-mass interval i is calculated as $N_i/(\varepsilon_i L_i)$. The number of selected events (N_i) for each $p\bar{p}$ invariant-mass interval after background subtraction is listed in Table III. The values of the L_i (Table III) have been obtained by integration of $W(s, x)$ from Refs. [4, 5] over each invariant-mass interval. They can be calculated also using the Phokhara event generator [7]. The results of the two calculations agree within 0.5%, which coincides with the estimated theoretical accuracy of the Phokhara generator [7]. The obtained values of the $e^+e^- \rightarrow p\bar{p}$ cross section are listed in Table III. For the invariant-mass intervals 3.0–3.2 GeV/c^2 and 3.6–3.8 GeV/c^2 we quote the nonresonant cross sections with the respective J/ψ and $\psi(2S)$ contributions excluded. The quoted errors are statistical, as obtained from the uncertainty in the number of selected $p\bar{p}\gamma$ events. The systematic uncertainty is independent of invariant mass and is equal to 4%. It includes the statistical error of the detection efficiency (2%), the uncertainty of the efficiency correction (3.3%), the uncertainty in the integrated luminosity (1%), and an uncertainty in the ISR luminosity (0.5%). The model uncertainty due to the unknown $|G_E/G_M|$ ratio (see Fig. 8) is about 15% at 3 GeV/c^2 , decreases to 5% at 4.5 GeV/c^2 , and does not exceed 5% at higher values. The measured $e^+e^- \rightarrow p\bar{p}$ cross section is shown in Fig. 10 together

TABLE III: The $p\bar{p}$ invariant-mass interval ($M_{p\bar{p}}$), number of selected events (N) after background subtraction, detection efficiency (ε), ISR luminosity (L), measured $e^+e^- \rightarrow p\bar{p}$ cross section ($\sigma_{p\bar{p}}$), and the proton magnetic form factor ($|G_M|$). The quoted uncertainties are statistical. The systematic uncertainty is 4% for the cross section, and 2% for the form factor. The model uncertainty for the cross section (form factor) is 15 (8)% at 3 GeV, decreases to 5 (3)% at 4.5 GeV, and does not exceed 5(3)% at higher values.

$M_{p\bar{p}}$ (GeV/ c^2)	N	ε (%)	L (pb $^{-1}$)	$\sigma_{p\bar{p}}$ (pb)	$ G_M $
3.0–3.2	33.0 ± 7.0	1.45	271	8.4 ± 1.8	$0.0310^{+0.0031}_{-0.0035}$
3.2–3.4	30.0 ± 5.7	2.69	292	3.8 ± 0.7	$0.0221^{+0.0020}_{-0.0022}$
3.4–3.6	30.0 ± 5.6	3.95	314	2.42 ± 0.45	$0.0186^{+0.0017}_{-0.0018}$
3.6–3.8	16.4 ± 5.1	4.97	337	0.98 ± 0.30	$0.0124^{+0.0018}_{-0.0021}$
3.8–4.0	15.0 ± 4.0	5.79	361	0.72 ± 0.19	$0.0112^{+0.0014}_{-0.0016}$
4.0–4.5	11.0 ± 3.5	6.54	1018	0.165 ± 0.053	$0.0058^{+0.0009}_{-0.0010}$
4.5–5.5	4.0 ± 2.3	8.62	2637	0.018 ± 0.010	$0.0022^{+0.0006}_{-0.0008}$
5.5–6.5	0.6 ± 1.1	10.79	4079	0.0014 ± 0.0025	$0.0007^{+0.0005}_{-0.0007}$

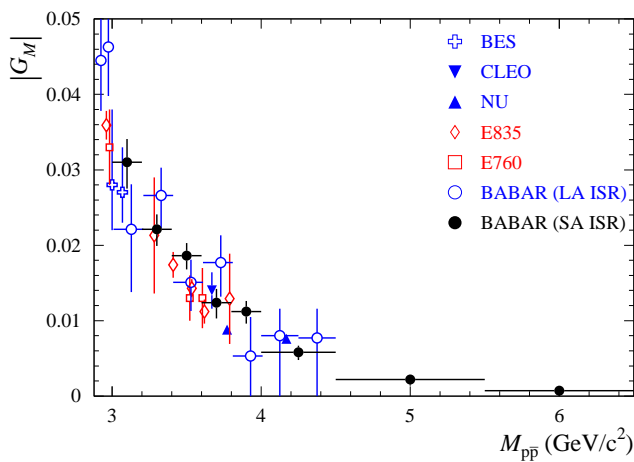


FIG. 11: The proton magnetic form factor measured in this analysis [BABAR (SA ISR)] and in other experiments: BES [9], CLEO [10], NU [11], E835 [13], E760 [12], BABAR (LA ISR) [2]

with the results of previous e^+e^- measurements.

The values of the proton magnetic form factor are obtained using Eq. (3) under the assumption that $|G_E| = |G_M|$. They are listed in Table III and shown in Fig. 11 (linear scale) and in Fig. 12 (logarithmic scale). It is seen that our results are in good agreement with the results from other experiments. The curve in Fig. 12 is the result of a fit of the asymptotic QCD dependence of the proton form factor [14], $|G_M| \sim \alpha_s^2(M_{p\bar{p}}^2)/M_{p\bar{p}}^4 \sim D/(M_{p\bar{p}}^4 \log^2(M_{p\bar{p}}^2/\Lambda^2))$, to all the existing data with $M_{p\bar{p}} > 3$ GeV/ c^2 , excluding the two points from Ref. [11]. Here $\Lambda = 0.3$ GeV and D is a free fit parameter. The data are well described by this function, with $\chi^2/\nu = 17/24$, where ν is the number of degrees of freedom. Including the points from Ref. [11] in the fit increases χ^2/ν to 54/26.

In Fig. 12 we also show the space-like $|G_M|$ data

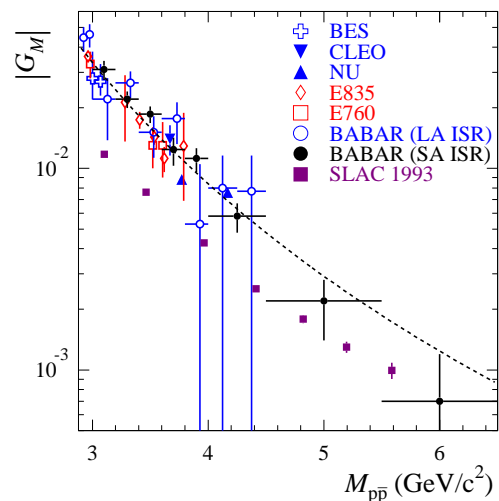


FIG. 12: The proton magnetic form factor measured in this analysis [BABAR (SA ISR)] and in other experiments: BES [9], CLEO [10], NU [11], E835 [13], E760 [12], BABAR (LA ISR) [2]. Points denoted by “SLAC 1993” represent data on the space-like magnetic form factor obtained in ep scattering [26] as a function of $\sqrt{-q^2}$, where q^2 is the momentum transfer squared. The curve is the result of the QCD-motivated fit described in the text.

(“SLAC 1993” points) obtained in Ref. [26]. The QCD prediction is that the space- and time-like asymptotic values be the same. In the region from 3.0 to 4.5 GeV/ c^2 the value of the time-like form factor is about two times larger than that of the space-like one. Our points above 4.5 GeV/ c^2 give some indication that the difference between time- and space-like form factors may be decreasing, although our measurement uncertainties are large in this region.

VIII. SUMMARY

The process $e^+e^- \rightarrow p\bar{p}\gamma$ has been studied in the $p\bar{p}$ invariant-mass range from 3.0 to 6.5 GeV/ c^2 for events with an undetected ISR photon emitted close to the collision axis. From the measured $p\bar{p}$ invariant-mass spectrum we extract the $e^+e^- \rightarrow p\bar{p}$ cross section, and determine the magnitude of the magnetic form factor of the proton. This is the first measurement of the proton form factor at $p\bar{p}$ invariant masses higher than 4.5 GeV/ c^2 . The observed strong decrease of the form factor for $M_{p\bar{p}} < 4.5$ GeV/ c^2 agrees with the asymptotic dependence $\alpha_s^2(M_{p\bar{p}}^2)/M_{p\bar{p}}^4$ predicted by QCD. There is some indication of an even faster decrease for $M_{p\bar{p}} > 4.5$ GeV/ c^2 .

The branching fractions for the decays $J/\psi \rightarrow p\bar{p}$ and $\psi(2S) \rightarrow p\bar{p}$ have been measured, and the values

$$\begin{aligned} \mathcal{B}(J/\psi \rightarrow p\bar{p}) &= (2.33 \pm 0.08 \pm 0.09) \times 10^{-3}, \\ \mathcal{B}(\psi(2S) \rightarrow p\bar{p}) &= (3.14 \pm 0.28 \pm 0.18) \times 10^{-4} \end{aligned} \quad (10)$$

have been obtained. These values are in agreement with previous measurements.

IX. ACKNOWLEDGMENTS

We are grateful for the extraordinary contributions of our PEP-II colleagues in achieving the excellent luminos-

ity and machine conditions that have made this work possible. The success of this project also relies critically on the expertise and dedication of the computing organizations that support BABAR. The collaborating institutions wish to thank SLAC for its support and the kind hospitality extended to them. This work is supported by the US Department of Energy and National Science Foundation, the Natural Sciences and Engineering Research Council (Canada), the Commissariat à l'Énergie Atomique and Institut National de Physique Nucléaire et de Physique des Particules (France), the Bundesministerium für Bildung und Forschung and Deutsche Forschungsgemeinschaft (Germany), the Istituto Nazionale di Fisica Nucleare (Italy), the Foundation for Fundamental Research on Matter (The Netherlands), the Research Council of Norway, the Ministry of Education and Science of the Russian Federation, Ministerio de Ciencia e Innovación (Spain), and the Science and Technology Facilities Council (United Kingdom). Individuals have received support from the Marie-Curie IEF program (European Union) and the A. P. Sloan Foundation (USA).

-
- [1] B. Aubert *et al.* (BABAR Collaboration), Phys. Rev. D **73**, 012005 (2006).
- [2] J. P. Lees *et al.* (BABAR Collaboration), Phys. Rev. D **87**, 092005 (2013).
- [3] V. P. Druzhinin, S. I. Eidelman, S. I. Serednyakov, and E. P. Solodov, Rev. Mod. Phys. **83**, 1545 (2011).
- [4] O. Nicosini and L. Trentadue, Phys. Lett. B **196**, 551 (1987).
- [5] F. A. Berends, W. L. van Neerven and G. J. H. Burgers, Nucl. Phys. B **297**, 429 (1988) [Erratum-ibid. B **304**, 921 (1988)].
- [6] M. Benayoun, S. I. Eidelman, V. N. Ivanchenko and Z. K. Silagadze, Mod. Phys. Lett. A **14**, 2605 (1999).
- [7] H. Czyz, A. Grzelinska, J. H. Kuhn and G. Rodrigo, Eur. Phys. J. C **39**, 411 (2005).
- [8] A. B. Arbuzov and T. V. Kopylova, JHEP **1204**, 009 (2012).
- [9] M. Ablikim *et al.* (BES Collaboration), Phys. Lett. B **630**, 14 (2005).
- [10] T. K. Pedlar *et al.* (CLEO Collaboration), Phys. Rev. Lett. **95**, 261803 (2005).
- [11] K. K. Seth *et al.*, Phys. Rev. Lett. **110**, 022002 (2013).
- [12] T. A. Armstrong *et al.* (E760 Collaboration), Phys. Rev. Lett. **70**, 1212 (1993).
- [13] M. Ambrogiani *et al.* (E835 Collaboration), Phys. Rev. D **60**, 032002 (1999); M. Andreotti *et al.* (E835 Collaboration), Phys. Lett. B **559**, 20 (2003).
- [14] V. L. Chernyak and A. R. Zhitnitsky, JETP Lett. **25**, 510 (1977); G. P. Lepage and S. J. Brodsky, Phys. Rev. Lett. **43**, 545 (1979).
- [15] J. P. Lees *et al.* (BABAR Collaboration), Nucl. Instr. and Methods Phys. Res., Sect. A **726**, 1 (2013).
- [16] B. Aubert *et al.* (BABAR Collaboration), Nucl. Instr. and Methods Phys. Res., Sect. A **479**, 1 (2002); B. Aubert *et al.* (BABAR Collaboration), Nucl. Instr. and Methods Phys. Res., Sect. A (in press), available online at <http://dx.doi.org/10.1016/j.nima.2013.05.107>.
- [17] V. L. Chernyak, A. R. Zhitnitsky and V. G. Serbo, JETP Lett. **26**, 594 (1977) [Pisma Zh. Eksp. Teor. Fiz. **26**, 760 (1977)].
- [18] S. Jadach, W. Placzek and B. F. L. Ward, Phys. Lett. B **390**, 298 (1997).
- [19] B. Aubert *et al.* (BABAR Collaboration), Phys. Rev. D **81**, 092003 (2010).
- [20] T. Sjöstrand, Comput. Phys. Commun. **82**, 74 (1994).
- [21] S. Agostinelli *et al.* (Geant4 Collaboration), Nucl. Instr. and Methods Phys. Res., Sect. A **506**, 250 (2003).
- [22] M. Ablikim *et al.* (BESIII Collaboration), Phys. Rev. D **86**, 032014 (2012).
- [23] M. Ambrogiani *et al.* (E835 Collaboration), Phys. Lett. B **610**, 177 (2005).
- [24] M. Ablikim *et al.* (BES Collaboration), Phys. Lett. B **648**, 149 (2007).
- [25] J. Beringer *et al.* (Particle Data Group), Phys. Rev. D

86, 010001 (2012).

[26] A. F. Sill *et al.*, Phys. Rev. D **48**, 29 (1993).